RESEARCH

Using a flat-panel detector in high resolution cone beam CT for dental imaging

R Baba*[,1], K Ueda[2] and M Okabe[2]

[1]Central Research Laboratory, Hitachi, Ltd., Tokyo, Japan; [2]Research & Development Center, Hitachi Medical Corporation, Chiba, Japan

Objectives: Cone beam CT (CBCT) requires a two-dimensional X-ray detector. In the several CBCT systems developed for dental imaging, detection has been by the combination of an X-ray image intensifier and charge-coupled device (CCD) camera. In this paper, we propose a new CBCT system in which the detector is of the flat-panel type and evaluate its performance in dental imaging.
Methods: We developed a prototype CBCT that has a flat-panel-type detector. The detector consists of a CsI scintillator screen and a photosensor array. First, the flat panel detector and image intensifier detector were compared in terms of the signal-to-noise ratio (SNR) of projected images. We then used these data and a theoretical formula to evaluate noise in reconstructed images. Second, reconstructed images of a bar pattern phantom were obtained as a way of evaluating the spatial resolution. Then, reconstructed images of a skull phantom were obtained.
Results: The SNR of the developed system was 1.6 times as high as that of a system with an image intensifier detector of equal detector pitch. The system was capable of resolving a 0.35 mm pattern and its field of view almost completely encompassed that of an image intensifier detector which is used in dentomaxillofacial imaging. The fine spatial resolution of the detector led to images in which the structural details of a skull phantom were clearly visible.
Conclusions: The system's isotropically fine resolution will lead to improved precision in dental diagnosis and surgery. The next stage of our research will be the development of a flat panel detector system with a high frame acquisition rate.
Dentomaxillofacial Radiology (2004) **33,** 285–290. doi: 10.1259/dmfr/87440549

Keywords: imaging, three-dimensional; tomography, X-ray computed; surgery, oral

Introduction

Cone beam computed tomography (CBCT) requires a two-dimensional (2D) X-ray detector and a conical or pyramidal X-ray beam. Along with the 2D fluoroscopic and radiographic functions of the basic hardware, the acquisition of a full set (*i.e.* a set that covers 360°) of projection images during a single rotation scan plus computer processing allows us to reconstruct isotropically fine spatial resolution three-dimensional (3D) images. The pioneering CBCT systems were developed for application in angiography.[1-4]

A system in which an X-ray image intensifier and charge-coupled device (CCD) television camera act as the detector has been developed; this has been shown to be an effective aid for diagnosis, surgical planning and explanation of orthopaedic and angiographic procedures to patients.[5-7] More recently, a system in which the patient sits on a chair and the X-ray tube and detector revolve in a horizontal plane around the patient have been developed for dentomaxillofacial imaging.[8,9] The system can produce thin slice images, maximum intensity projection (MIP) images, rendered images and panoramic images from an internal 3D representation, thus providing a comprehensive range of high quality dental images. In the several CBCT systems that have been developed for dental imaging, detection has been achieved by the combination of an X-ray image intensifier and CCD camera.[8-10] Recently, a flat-panel-type detector has begun to be used.[11,12]

In this paper, we propose a new CBCT system in which the detector is of the flat panel type and compare the performance of the two detector types in dental imaging.[13]

Methods

We developed two experimental setups for comparative evaluation of the two detector types in CBCT. Projected images of the subject on each detector were magnified by about 1.5 times. In the flat panel detector system, the X-ray source and detector are stationary and the subject is rotated in the horizontal plane by a turntable (Figure 1a). In the image intensifier detector system, the subject is stationary, and the X-ray source and detector revolve around the subject in the horizontal plane (Figure 1b). Equivalent images are obtained by both methods. The projected images are obtained during a 360° rotation scan. Reconstruction processing is performed by using the Feldkamp algorithm with the standard Shepp and Logan filter.[14]

In the flat panel detector (provided by Varian Medical Systems, Inc., Palo Alto, CA), the sensor elements are produced in a thin film of amorphous silicon (a-Si) and a large detector is thus realisable. The flat panel detector consists of a CsI scintillator screen and a photosensor array (Figure 2a). The photosensor array consists of arrayed photodiodes and switching devices. The scintillator converts an X-ray beam into an optical signal, which the photodiode converts to an electrical signal, which is in turn read out by the switching device array. The flat panel detector does not generate veiling glare or distortion in the image, and has a smaller detector pitch than an image intensifier detector.[15-17] The flat panel detector provides us with a square field of view (FOV). However, the flat panel detector is unlike the image intensifier detector in that it does not have an optical iris as a direct means for adjustment; this makes it difficult to prevent saturation of the pixels. Correction for saturated pixels, defective pixels, offsets, and the sensitivity of the detector is applied in the new system and reduces the intensity of streak and ring artefacts in reconstructed images. The flat panel detector has three operating modes: a 1×1 non-binning mode, a 2×2 binning mode, and a 4×4 binning mode (Table 1).
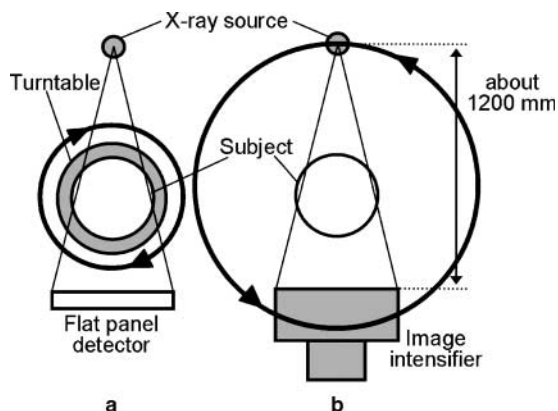

Figure 1 Experimental set-ups (top view): (a) flat panel detector system; (b) image intensifier detector system
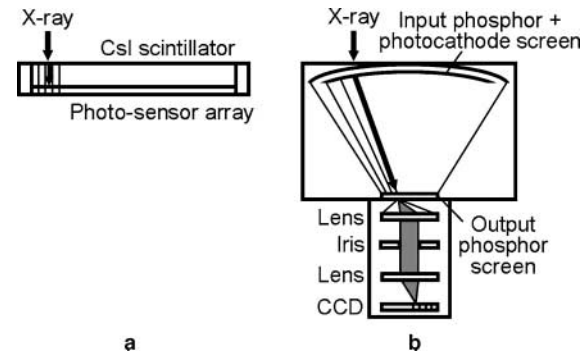

Figure 2 Components of the detectors: (a) flat panel detector; (b) image intensifier detector

All modes provide the same FOV, but the detector pitch of the 2×2 and 4×4 binning modes is twice and four times, respectively, the pitch in the 1×1 non-binning mode.

The image intensifier detector consists of a 9″ X-ray image intensifier, optics and a CCD television camera (Figure 2b). The X-ray beam is converted to an optical signal by the input phosphor screen; this signal is in turn converted to electrons by the photocathode screen. Electrons are accelerated by the electric field inside the image intensifier and converted back to an optical signal at the output phosphor screen. The intensity of the optical signal is adjusted by the optical iris; the signal is then detected by the CCD. The read-out image includes geometrical distortion and a blurring component of veiling glare generated by the image intensifier. This detector's FOV is circular. In this system, correction for the offset and sensitivity of the sensors, and the distortion of the detector is applied to reduce the intensity of artefacts in the reconstructed image. The image intensifier detector has three imaging modes: a 4.5″ mode, 7″ mode and 9″ mode (Table 1). The FOV differs with the mode. The detector pitch in the 4.5″ mode is the minimum, *i.e.* fits the minimum FOV, while that in the 9″ mode is the maximum, *i.e.* fits the maximum FOV.

The flat panel detector in the 2×2 binning mode has a 0.254 mm detector pitch and acquires projected images that consist of 768×960 12-bit pixels at 15 frames s^{-1}. The image intensifier detector in the 4.5″ mode has a 0.239 mm detector pitch and acquires projected images that consist of 512×512 12-bit pixels at 30 frames s^{-1}. The pitch of this detector in the 9″ mode is 0.438 mm pitch; acquisition is as in the 4.5″ mode. The flat panel detector has a larger FOV than the image intensifier detector in the 4.5″ mode or 7″ mode; its FOV is, in fact, almost equal to that of the image intensifier detector in the 9″ mode (Figure 3).

The flat panel detector was evaluated in the 2×2 binning mode. This mode was selected because the pitch of the detector is then almost equal to that of the image intensifier detector in 4.5″ mode and its FOV is almost equal to that of the image intensifier detector in 9″ mode. Thus, this mode provides the combination of small detector pitch and large FOV that is suitable for dentomaxillofacial imaging.

First, the two detectors were compared in terms of the signal-to-noise ratio (SNR) of projected images. We then

Table 1 Parameters of the detectors

Mode	Flat panel detector			Image intensifier detector		
	1 × 1 no binning	*2 × 2 binning*	*4 × 4 binning*	*4.5″*	*7″*	*9″*
Detector pitch (mm)	0.127	0.254	0.508	0.239	0.344	0.438
Measured image matrix (pixel)	1536 × 1920	768 × 960	384 × 480	512 × 512	512 × 512	512 × 512
Detector field of view (mm)	185 × 244	185 × 244	185 × 244	φ122	φ176	φ224
ADC bit number (bit)	12	12	12	12	12	12
Frame rate (frame s^{-1})	4	15	30	30	30	30

ADC, apparent diffusion coefficient

Figure 3 Field of view of the detectors

Figure 4 Signal-to-noise ratio (SNR) of projected images
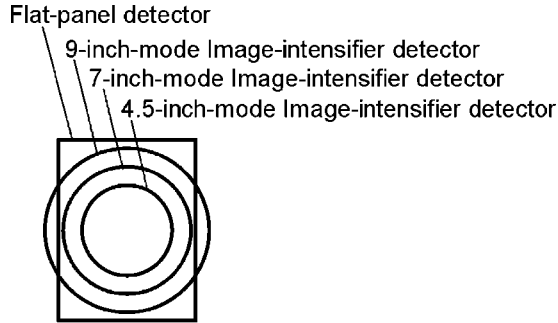
used these data and a theoretical formula to evaluate noise in reconstructed images. Second, reconstructed images of a bar pattern phantom were obtained as a way of evaluating the spatial resolution. Here, the image obtained by the flat panel detector was compared with that obtained by the image intensifier detector in 4.5″ mode, because this mode provides the smallest pitch available to the image intensifier detector. Reconstructed images of a skull phantom were then obtained. Here, images obtained by the flat panel detector were compared with those obtained by the image intensifier detector in 9″ mode, since this mode provides the largest FOV available to the image intensifier detector, and is capable covering the whole skull.

Results

Noise in reconstructed images
Projected images from the flat panel detector in 2 × 2 binning mode (0.254 mm detector pitch, 15 frames s^{-1} frame rate) and the image intensifier detector in 4.5″ mode (0.239 mm detector pitch, 30 frames s^{-1} frame rate) were evaluated for noise. The SNR was measured at a 120 kV X-ray tube voltage (Figure 4). Measured SNR values for the former and latter detectors are plotted as ▲ and •, respectively. The horizontal axis shows X-ray dose per pixel as measured at the surface of the detector. These measured data approximate the equation for the SNR of each detector. The equation consists of a first term that is proportional to the X-ray dose incident on the detector and a second term proportional to the square of this X-ray dose. The SNR of the flat panel detector calculated by using the equation is plotted as a solid line. The SNR of the image intensifier detector as calculated by using the equation is plotted as a dashed line. The lines fit the measured data well. Figure 4 shows that the projected image from the flat
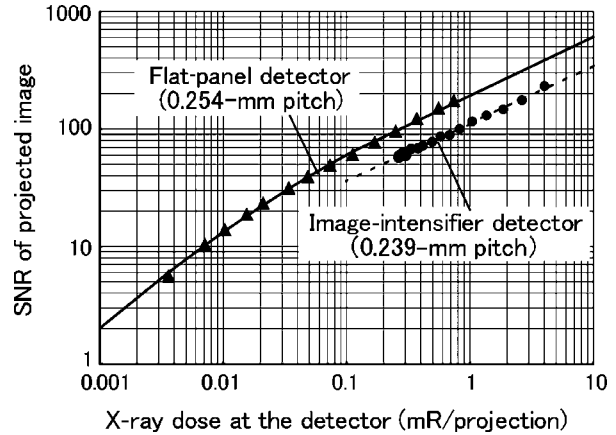
panel detector has an SNR 1.72 times that of the image intensifier detector.

According to the Feldkamp algorithm, the noise of a reconstructed image is given by Equation (1).

$$\mathrm{sd} = \sqrt{\left(\frac{a}{n}\right)^2 \cdot \sum_{i=1}^{n} \sum_{k=-\infty}^{\infty} \left\{\left(\frac{1}{\mathrm{SNR}_i}\right)^2 \cdot w(k)^2\right\} \cdot c}$$

$$= \sqrt{\left(\frac{a}{n}\right)^2 \cdot \sum_{k=-\infty}^{\infty} w(k)^2 \sum_{i=1}^{n} \left(\frac{1}{\mathrm{SNR}_i}\right)^2 \cdot c} \qquad (1)$$

Here, sd means the standard deviation of the voxels of the reconstructed image, a is the detector pitch as projected on the subject (mm), n the number of projected images, SNR_i the signal-to-noise ratio of the ith projected image, $w(k)$ the convolution filter and c is the coefficient for transformation from X-ray absorption coefficient (mm^{-1}) to CT number (HU). When the Shepp and Logan filter with linear interpolation is in use, the convolution filter is as given by Equation (2).

$$\sum_{k=-\infty}^{\infty} w(k)^2 = \frac{1}{a} \cdot \int_{-\infty}^{\infty} W(f)^2 df$$

$$= \frac{1}{a} \cdot \int_{-\frac{1}{2 \cdot a}}^{\frac{1}{2 \cdot a}} \frac{1}{a^2 \cdot (\pi \cdot a \cdot f)^4} \cdot \sin^6(\pi \cdot a \cdot f) df$$

$$= 0.440 \cdot \frac{1}{2 \cdot a^4} \qquad (2)$$

Here, 0.440 is the coefficient obtained for this filter. Substituting Equation (2) into Equation (1) gives us Equation (3).

$$sd = \sqrt{\frac{a^2}{n} \cdot \left(0.440 \cdot \frac{1}{2a^4}\right) \cdot \frac{1}{n} \cdot \sum_{i=1}^{n} \left(\frac{1}{SNR_i}\right)^2 \cdot c} \quad (3)$$

When the subject is assumed to be a cylinder, the SNR of the projected image is as given by Equation (4).

$$\frac{1}{n} \cdot \sum_{i=1}^{n} \left(\frac{1}{SNR_i}\right)^2 = \left(\frac{1}{SNR}\right)^2 \quad (4)$$

Here, SNR indicates the signal-to-noise ratio of the projected image. With Equation (4), Equation (3) becomes Equation (5).

$$sd = \sqrt{\frac{0.440}{2 \cdot n}} \cdot \frac{c}{a \cdot SNR} \quad (5)$$

The noise of the reconstructed image is given by Equation (5), *i.e.* is inversely proportional to the detector pitch and SNR of the projected image. Table 1 shows that the detector pitch of the flat panel detector is 1.06 times that of the image intensifier detector. In that case, Figure 4 shows that the projected images of the flat panel detector have SNR values 1.72 times as high as use of the image intensifier detector. As the SNR is proportional to the detector pitch, the SNR of the flat panel detector when it has the same pitch as the image intensifier detector will be 1.62 times that of the image intensifier detector. Thus, given equal detector pitch, the reconstructed image of the flat panel detector is presumed to have a noise level 1.62 times lower than that of the image intensifier detector.

Spatial resolution of reconstructed images
We evaluated the spatial resolution of reconstructed images obtained by the flat-panel detector in 2 × 2-binning mode (0.254 mm detector pitch, 15 frames s^{-1} frame rate) and the image intensifier detector in 4.5″ mode (0.239 mm detector pitch, 30 frames s^{-1} frame rate). The spatial resolution was evaluated by measuring a high-contrast bar pattern in a 165 mm diameter cylindrical water phantom. The pattern was set in a plane perpendicular to the axis of rotation for the evaluation of axial images and in a plane parallel to the same axis for the evaluation of coronal images.

When the detector pitch of the flat panel detector was 0.254 mm, a 0.35 mm bar pattern was resolved in both axial and coronal images extracted from the respective reconstructed images (120 kV tube voltage, 460.8 mAs total dose, 576 frame projection, 0.169 mm voxel pitch) (Figure 5a, b). The 0.35 mm pattern was also resolved in the reconstructed image of the image intensifier detector with a detector pitch of 0.239 mm (Figure 5c). The respective reconstructed images had roughly equal spatial resolution. CBCT using the flat panel detector had isotropic spatial resolution equal to that of the image intensifier detector with the smallest detector pitch, *i.e.* in the imaging mode that is used for dentomaxillofacial imaging.

Skull phantom imaging
A skull phantom in water was imaged by the flat panel detector system in 2 × 2-binning mode (0.254 mm detector pitch, 15 frames s^{-1} frame rate) and by the image intensifier detector system in 9″ mode (0.438 mm detector pitch, 30 frames s^{-1} frame rate). The reconstructed image obtained with the flat panel detector system had a cylindrical FOV with 0.215 mm voxel pitch. The reconstructed image obtained with the image intensifier detector system had a globular FOV with 0.293 mm voxel pitch. Reconstructed images covered the skull.

In the flat panel detector system, correction for defective or saturated pixels and the offset, and sensitivity of detector elements was applied to the projected images, so that neither streak nor ring artefacts were found in the reconstructed images (120 kV tube voltage, 214.8 mAs total dose, 288 frame projection) (Figure 6a). The details of the skull's structures were more clearly depicted by the flat panel detector system than by the image intensifier detector system (Figure 6b, c). The reconstructed images obtained by the flat panel detector system had high resolution on all planes (axial, coronal and sagittal, Figure 6a and Figure 7a, b). The surface of the bone appears smooth in the volume rendered image because this system had a high spatial resolution and little blurring (Figure 7c). Even the thin bone in the nasal cavity is distinguishable.

Conclusions and discussion

The evaluation showed that, given equal detector pitch, reconstructed images obtained with the flat panel detector
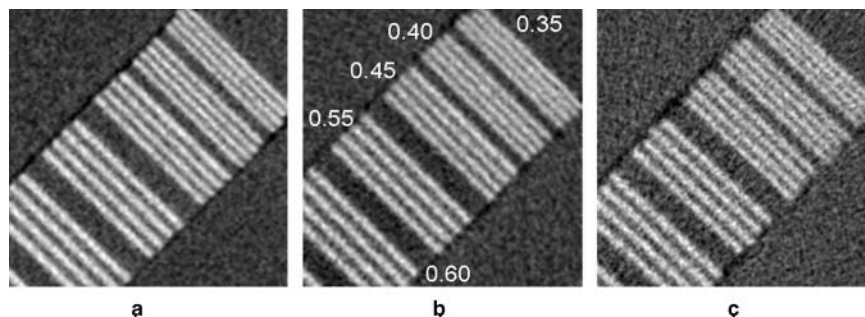

Figure 5 Three-dimensional images of a high-contrast pattern: (a) coronal image by flat panel detector (2 × 2-binning mode); (b) axial image by flat panel detector (2 × 2-binning mode); (c) axial image by image intensifier detector (4.5″ mode)
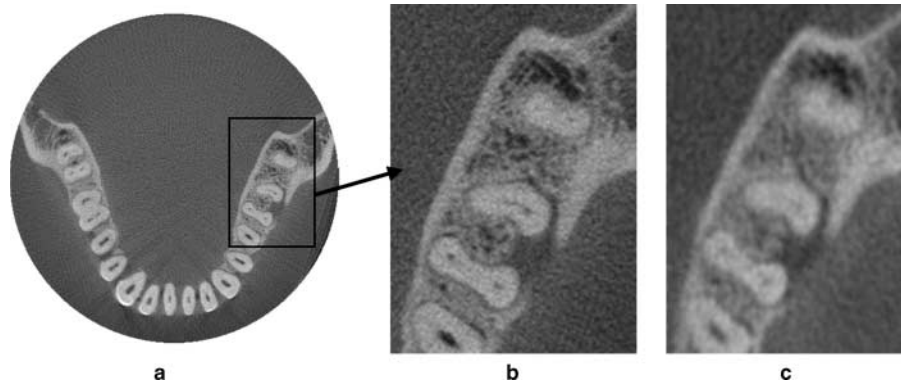
Figure 6 Axial images of a skull phantom: (a) flat panel detector system (2 × 2-binning mode); (b) flat-panel detector system (2 × 2-binning mode); (c) image intensifier detector system (9″ mode)
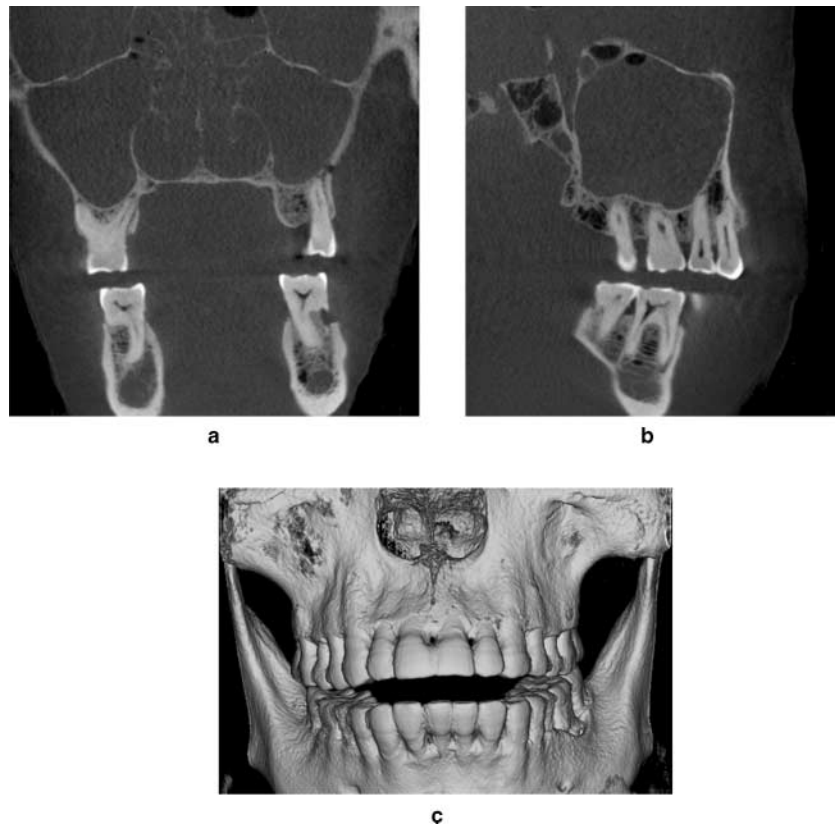

Figure 7 Three-dimensional images of a skull phantom obtained by the flat panel detector system: (a) coronal image; (b) sagittal image; (c) volume rendered image

have less noise than those obtained with the image intensifier detector. The flat panel detector system we developed had spatial resolution equal to that of the image intensifier detector system in its smallest detector pitch mode, and our system's FOV was almost equal to that of the image intensifier detector system at its largest FOV, that is, in the operating mode used for dentomaxillofacial imaging. The high quality of reconstructed images obtained with the CBCT system using a flat panel detector offers improved precision in dentistry, for both diagnosis and surgery.

The next stage of our research will be the development of a flat panel detector CBCT with a high frame-acquisition rate. We also intend to improve fineness of contrast resolution as this will be important if we are to expand the application of CBCT. We are currently evaluating a new prototype CBCT in which the detector is of this type.

References

1. Ritman EL, Kinsey JH, Robb RA, Gilbert BK, Harris LD, Wood EH. Three-dimensional imaging of heart, lungs, and circulation. *Science* 1980; **210:** 273–280.

2. Ning R, Kruger RA. Computer simulation of image intensifier-based computed tomography detector: vascular application. *Med Phys* 1988; **15:** 188–192.

3. Saint-Felix D, Picard C, Ponchut C, Romeas R, Rougee A, Troussert Y. Three dimensional X-ray angiography: first in vivo results with a new system. *Proc SPIE* 1993; **1897:** 90–98.

4. Ning R, Wang X, Conover DL, Tang X. An image intensifier-based volume tomographic angiography imaging system. *Proc SPIE* 1997; **3032:** 238–246.

5. Baba R, Ueda K, Ueki H, Umetani K. Ellipsoid scan: chest cone-beam CT with a large ellipsoidal view field using a 16-inch X-ray image intensifier. *Proc SPIE* 1999; **3032:** 349–357.

6. Baba R, Ueda K, Kawai H, Kuba A, Takagi H. Development of three-dimensional imaging method with cone-beam X-ray. *MEDIX* 1999; **31:** 42–47.

7. Baba R, Ueda K, Kuba A, Kohda E, Shiraga N, Sanmiya T. Development of a subject-standing-type cone-beam computed tomography for chest and orthopedic imaging. *Front Med Biol Eng* 2001; **11:** 177–189.

8. Seo K, Yamamoto K, Ueno K, Tanaka K, Matsuoka M, Okabe K, et al. Development of dentomaxillofocial conebeam X-ray CT system model CB MercuRay. *MEDIX* 2002; **37:** 40–45.

9. Maki K, Usui T, Kubot M, Nakano H, Shibasaki Y, Araki K, et al. Application of cone-beam X-ray CT in dento-maxillofacial region. *Proc CARS* 2002; 1–5.

10. Arai Y, Tammisalo E, Iwai K, Hashimoto K, Shinoda K. Development of a compact computed tomographic apparatus for dental use. *Dentmaxillofac Radiol* 1999; **28:** 245–248.

11. Sukovic P, Brooks S, Perez L, Clinthorne NH. DentoCAT™ – A novel design of a cone beam CT scanner for dentomaxillofacial imaging: introduction and preliminary results. *Proc CARS* 2001; 659–664.

12. Sukovic P. Cone beam computed tomography in craniofacial imaging. *COAST* 2002; 9 (Abstr).

13. Baba R, Ueda K, Kadomura T. High-resolution FPD cone-beam CT for dental and orthopedic surgery. *Radiology* 2002; **225(P):** 194 (Abstr).

14. Feldkamp LA, Davis LC, Kress JW. Practical cone-beam algorithm. *J Opt Soc Am A* 1984; **1:** 612–619.

15. Colbeth RE, Allen MJ, Day DJ, Gilblom DL, Harris R, Job ID, et al. Flat panel imaging system for fluoroscopy applications. *Proc SPIE* 1998; **3336:** 376–387.

16. Yamada S, Umazaki H, Takahashi A, Honda M, Shiraishi K, Rudin S, et al. Image quality evaluation of a selenium-based flat-panel digital X-ray detector system based on animal studies. *Proc SPIE* 2000; **3977:** 429–436.

17. Granfors PR, Aufrichtig R. Performance of a 41×41-cm^2 amorphous silicon flat panel X-ray detector for radiographic imaging applications. *Med Phys* 2000; **27:** 1324–1331.